Performance evaluation of optical beamforming-based wideband antenna array

(Invited Paper)

Xingwei Ye (叶星炜), Bowen Zhang (张博文), Yamei Zhang (张亚梅), Dan Zhu (朱 丹), and Shilong Pan (潘时龙)*

Key Laboratory of Radar Imaging and Microwave Photonics, Ministry of Education, Nanjing University of Aeronautics and Astronautics, Nanjing 210016, China

**Corresponding author: pans@ieee.org*

Received September 19, 2016; accepted December 2, 2016; posted online December 21, 2016

A wideband-generalized pattern multiplication approach to evaluate the performance of an optical beamforming-based wideband antenna array is proposed and experimentally demonstrated, which enables the far-field measurement of a large wideband array with a small anechoic chamber. Because the optimum reception of a wideband microwave signal is highly related to the time-domain distortions of the beamforming system, a correlation-receiver-based radiation pattern is applied to take the fidelity of the wideband signals into account. A four-element optical beamforming system is built to verify the feasibility of the proposed method. The results achieved by the proposed method agree well with the conventional direct measurements.

OCIS codes: 280.5110, 060.5625.

doi: 10.3788/COL201715.010013.

Optical beamforming, which is one of the most promising solutions to the beam-squint problem in wideband array antenna systems, such as high-resolution radars, electronic warfare systems, and the upcoming 5G mobile communication systems, has been a topic of interest in the last few decades[1–7]. Thanks to the intrinsic advantage of large instantaneous bandwidth brought by optical technologies, broadband and large-range true time delay (TTD) can be easily implemented in the optical domain[8–12]. Thus, complex waveforms with larger instantaneous bandwidth can be applied, which enables distinctive features such as better resolution for ranging[13], larger suppression of grating lobes[14,15], and higher speed in wireless communications[16,17]. For the optical beamforming-based wideband antenna array, it is of great importance to know what the output signal at an arbitrary radiation direction is for a given wideband input signal. However, the conventional way to characterize the antenna array is implemented by measuring the radiation patterns at a specific frequency or several discrete frequencies in an anechoic chamber[18,19], which cannot obtain the complete information of the antenna system at a wide bandwidth. To solve this problem, an integrated antenna pattern (IAP) is defined[20], which is the integration of the transmitted power at a radiation direction over the whole signal duration. The IAP maps the two-dimensional angle-time function to a one-dimensional angle function, which can be used to calculate the radio frequency (RF) energy at certain radiation directions for a given feeding waveform. However, information about the time-domain distortion of the wideband signal in the antenna and the optical beamforming network (OBFN) cannot be obtained. Because the optimum reception of a wideband microwave signal is highly related to the time-domain distortions[21], the wideband antenna system cannot be characterized by simply measuring the IAP.

Another challenge in evaluating the optical beamforming-based wideband antenna array is that the size of the required anechoic chamber is nearly proportional to the square of the scale of the antenna array. According to the antenna theory, for an antenna with a maximum overall dimension of D and a feeding wavelength of λ, the inner boundary of the far-field region is $2D^2/\lambda$[22]. If N antennas are arranged in a one-dimensional array, and the spacing between two adjacent antennas is d, the inner boundary should be larger than $2[(N-1)d]^2/\lambda$, indicating that a big anechoic chamber should be used, which would dramatically increase the cost in the optical beamforming research. Although the near-field or compact-range antenna measurement could be resorted, which requires only a small chamber, some special instruments, such as the planar scanner for near-field probing and the reflector for compact-range implementation, could also bring about an unaffordable cost. This might be a reason for the fact that radiation patterns in most works on optical beamforming were obtained through numerical simulation[23,24] rather than actual field measurement. Actually, the classical antenna theory has provided a pattern multiplication approach to enable field measurement of a large array with a small anechoic chamber[22]. In the pattern multiplication approach, the total far-field is equal to the field of a single element multiplied by the array factor, which is defined as the summation of the complex feeding amplitudes for all antenna elements. But, this approach can only be applied to achieving the radiation pattern at a single frequency.

In this Letter, a correlation-receiver-based radiation pattern measured by a generalized pattern multiplication approach is proposed to evaluate the performance of an optical beamforming-based wideband antenna array. The correlation-receiver-based radiation pattern assumes that the radiated signal at a radiation direction is received by a correlation receiver, and the maximum of the cross-correlation between the radiated signal and the feeding signal is adopted as the amplitude of the radiation pattern at that radiation direction[25]. Since the correlation receiver is assumed, the time-domain response of the antenna and the OBFN is taken into account, and its influence becomes observable. In addition, a generalized pattern multiplication approach is developed for wideband far-field measurement in which frequency is introduced as a new independent variable to the classical pattern multiplication approach. The frequency-dependent far-field radiation of a single antenna element is first measured, which requires only a small anechoic chamber. Then, the radiation feature of an antenna array in the band of interest is calculated by the summation of the complex feeding amplitudes for all antenna elements. Because the proposed method is developed for the wideband scenario, the wideband feature of optical beamforming can be studied and explored. A four-channel OBFN for feeding a four-element wideband antenna array is built to validate the proposed method. The feasibility of the generalized pattern multiplication approach is demonstrated and the sensitivity of the correlation-receiver-based pattern to the signal distortion in the time domain is studied.

Figure 1(a) shows the configuration of a typical one-dimensional optical beamforming-based antenna array in which an RF signal is multi-cast and independently controlled in terms of delay, phase, and amplitude with optical techniques in each channel of an OBFN. The electric field radiated by the antenna array is affected by both the

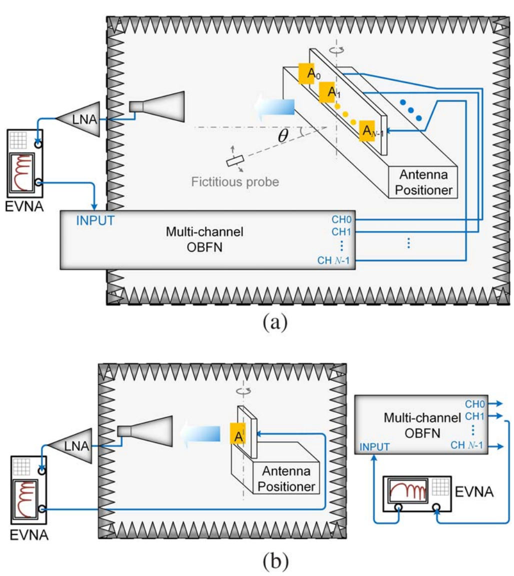

Fig. 1. Comparison of the two methods for the measurement of an antenna array: (a) direct measurement with a large anechoic chamber and (b) indirect measurement using a wideband-generalized pattern multiplication approach with a small chamber.

response of the OBFN and the radiation feature of the antenna elements. Using the superposition theorem and neglecting the mutual coupling between the antenna elements as well as all of the nonlinear effects, the signal probed at a constant distance in the far-field range and an observation angle of θ with respect to the broadside direction can be expressed as

$$\begin{aligned} S_R(\omega,\theta) &\propto \sum_n \Big\{ S_T(\omega)\cdot H_n(\omega)\cdot A_n(\omega,\theta) \\ &\quad \cdot \exp\left[-j\omega\frac{1}{c}d(n)\sin\theta\right]\Big\} \\ &= S_T(\omega)\cdot H_{\mathrm{SYS}}(\omega,\theta), \end{aligned} \tag{1}$$

where $S_T(\omega)$ is the spectrum of the feeding signal, $H_{\mathrm{SYS}}(\omega,\theta)$ is the system response that contains both the response of the OBFN and the radiation feature of the antenna elements, $H_n(\omega)$ is the frequency response of the nth channel in the OBFN, $A_n(\omega,\theta)$ is the radiation pattern of the nth antenna, $d(n)$ is the distance between the nth antenna and a reference point that determines the signal delay at the probe, c is the speed of light in vacuum, and ω, the angular frequency, is listed as an independent variable to adapt for the wideband scenario. Assume that the antennas are similar and are uniformly arranged, $H_{\mathrm{SYS}}(\omega,\theta)$ can be written as

$$\begin{aligned} &H_{\mathrm{SYS}}(\omega,\theta) \\ &\propto A(\omega,\theta)\cdot\left[\sum_n H_n(\omega)\cdot\exp\left(-j\omega\frac{nd}{c}\sin\theta\right)\right] \\ &+\sum_n\left\{A_{\Delta,n}(\omega,\theta)\cdot H_n(\omega)\cdot\exp\left(-j\omega\frac{nd}{c}\sin\theta\right)\right\}, \end{aligned} \tag{2}$$

where $A(\omega,\theta)$ is the average pattern of the antennas, $A_{\Delta,n}(\omega,\theta)$ is the deviation of the radiation feature for the nth antenna, and d is the uniform spacing between two adjacent antenna elements. In practice, $|A_{\Delta,n}(\omega,\theta)|$ is designed to be much smaller than $|A(\omega,\theta)|$, thus, Eq. (1) can be simplified to

$$S_R(\omega,\theta)\propto S_T(\omega)\cdot H_{\mathrm{SYS}}(\omega,\theta), \tag{3}$$

where

$$H_{\mathrm{SYS}}(\omega,\theta) = A(\omega,\theta)\cdot AF(\omega,\theta), \tag{4}$$

$$AF(\omega,\theta) = \sum_n H_n(\omega)\cdot\exp\left(-j\omega\frac{nd}{c}\sin\theta\right). \tag{5}$$

Equation (3) gives the definition of the *wideband-generalized pattern multiplication approach*. Compared with the classical pattern multiplication approach, the generalized one takes both the feeding waveform and the wideband responses into consideration, which can be applied in the wideband antenna array analysis. In addition, as can be seen from Eqs. (3) and (4), the total field radiated by the array is factorized into three terms: the spectrum of the feeding signal $S_T(\omega)$, the pattern of a single antenna $A(\omega,\theta)$, and the *frequency-dependent array factor* $AF(\omega,\theta)$, which is defined by Eq. (5). In practice, $S_T(\omega)$ is a known function, $A(\omega,\theta)$ can be measured by an electrical vector network analyzer (EVNA) in a small anechoic chamber, and $AF(\omega,\theta)$ can be achieved by measuring the response of each channel in the OBFN using the EVNA. As a result, the measurement schemes can be simplified to Fig. 1(b). It should be noted that when measuring $A(\omega,\theta)$ a receiving antenna and an optional low noise amplifier (LNA) might be employed. Their response $H_R(\omega)$ could affect the measurement accuracy. Fortunately, if an absolute-gain measurement[26] is conducted or if $H_R(\omega)$ performs close to an ideal delay line, the influence of the receiving antenna and the amplifier can be eliminated or neglected.

Although Eq. (3) can give the accurate radiation feature of an optical beamforming-based wideband antenna array, it is a two-dimensional frequency-angle function. To obtain the performance of the wideband antenna array in an intuitive way, the received signal from each observation angle is sent to a matched filter for correlation reception. The maximum of the cross-correlation between the radiated signal and the feeding signal is adopted as the amplitude of the radiation pattern at that angle. As such, a correlation-receiver-based radiation pattern, or *correlation-maximum pattern* (CMP), is obtained. Since the correlation receiver is sensitive to the time-domain distortions, the influence of the time-domain response of the antenna and the OBFN becomes observable.

Mathematically, the output waveform of the matched filter is given by

$$s_{\mathrm{cor}}(\tau,\theta) = \mathcal{F}^{-1}\{S_R(\omega,\theta)\cdot S_T^*(\omega)\} = \int_{-\infty}^{+\infty} s_R(t,\theta)\cdot s_T(t+\tau)\mathrm{d}t, \tag{6}$$

where $\mathcal{F}^{-1}\{\cdot\}$ denotes the inverse Fourier transformation, and $s_R(t,\theta)$ and $s_T(t)$ are the signals in the time domain. The CMP, i.e., the maximum of $s_{\mathrm{cor}}(\tau,\theta)$ at a certain observation angle θ, can be written as

$$\mathrm{CMP}(\theta) = \max_\tau\{s_{\mathrm{cor}}(\tau,\theta)\}. \tag{7}$$

For band-pass signals, the CMP can also be defined using the envelope of the correlation receiver output:

$$\widetilde{\mathrm{CMP}}(\theta) = \max_\tau\{|\tilde{s}_{\mathrm{cor}}(\tau,\theta)|\}. \tag{8}$$

Based on the definition of the CMP and the generalized pattern multiplication approach, the optical beamforming-based wideband antenna array can be characterized by using a process shown in Fig. 2.

To verify the feasibility of the proposed method, we first experimentally compare the $H_{\mathrm{SYS}}(\omega,\theta)$ defined in Eq. (2), which is directly measured in a anechoic chamber, and the simplified $H_{\mathrm{SYS}}(\omega,\theta)$ in Eq. (4), which is acquired by three

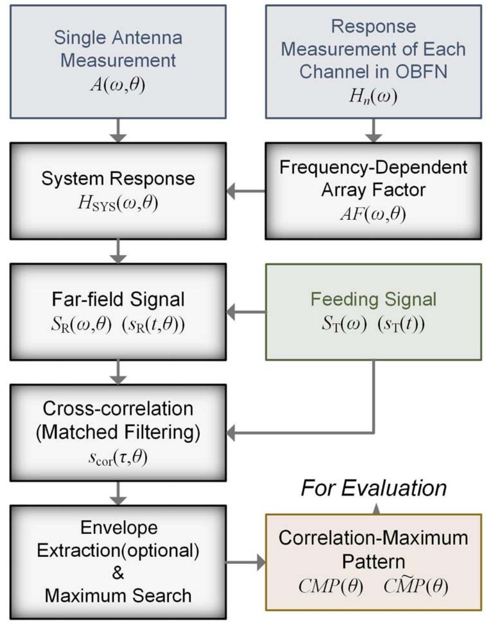

Fig. 2. Flow chart of the process for performance evaluation of the optical beamforming-based wideband antenna array.

steps: single-antenna-element measurement in a chamber, frequency response measurement of the OBFN using an EVNA, and post calculation using the proposed wideband-generalized pattern multiplication approach. The measurement setups are shown in Fig. 1. A four-channel OBFN is built with the schematic diagram shown in Fig. 3. An optical carrier from a laser source (Agilent N7714A) is sent to an electro-optic modulator (EOM) driven by a RF signal from an EVNA (Rohde & Schwarz ZVA67). After amplification in an erbium-doped fiber amplifier (EDFA), the modulated lightwave is equally divided into four channels in which the relative delays between the channels are adjusted by three optical variable delay lines (OVDL, General Photonics Inc.). The optical signals are then converted back to the RF domain in four photodetectors (PDs) for feeding a four-element X-band antenna array in which the spacing between two adjacent elements is 3 cm. In the anechoic chamber depicted in Fig. 3, the receiving horn antenna is placed 2.7 m away from the

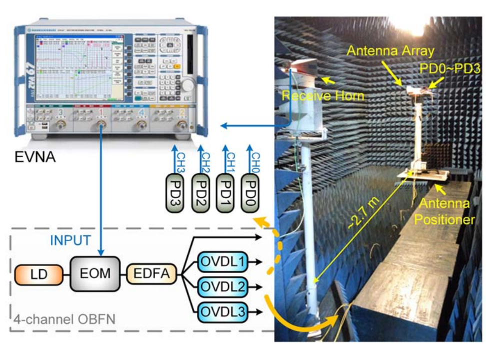

Fig. 3. Diagram of the optical TTD-based OBFN used in the experiment and a photograph of the experimental setup in anechoic chamber.

positioner that carries the antenna array under test, which is far enough to fit the far-field conditions of both the single antenna element and the four-element array. Signals captured by the receiving antenna are amplified by an 8–18 GHz LNA and then sent back to the EVNA. For the direct measurement, the four-antenna element in the array is simultaneously excited by RF signals from the PDs, while for the indirect measurement, the RF signal from each PD is immediately sent to the ENVA for the measurement of $H_n(\omega)$, and only one element in the array is excited by the RF output from the ENVA to measure $A(\omega,\theta)$.

In the experiment, the OVDLs are adjusted to orient the main lobe of the array to the directions of 0° and 45°. In addition, a random delay setting is applied to realize a none-main lobe scenario. System responses of the three configurations are shown in Fig. 4 in which the results of the direct measurement and the proposed indirect measurement are depicted in the left and right columns, respectively. Due to the fact that the pattern of one single antenna in the array reaches its maximum at around 0°, the array main lobe at 0° in Figs. 4(a) and 4(b) is more prominent than the 45°-main lobe in Figs. 4(c) and 4(d). For the same reason, the grating lobe caused by the large spacing of 3 cm, which is equal to the wavelength of a 10 GHz sine wave, prevails over the remote main lobe at an angle of 45°.

To compare the two-dimensional results in depth, several sectional drawings along both the frequency and the angle directions are plotted, as shown in Fig. 5. In addition, the CMPs of the three beamforming configurations

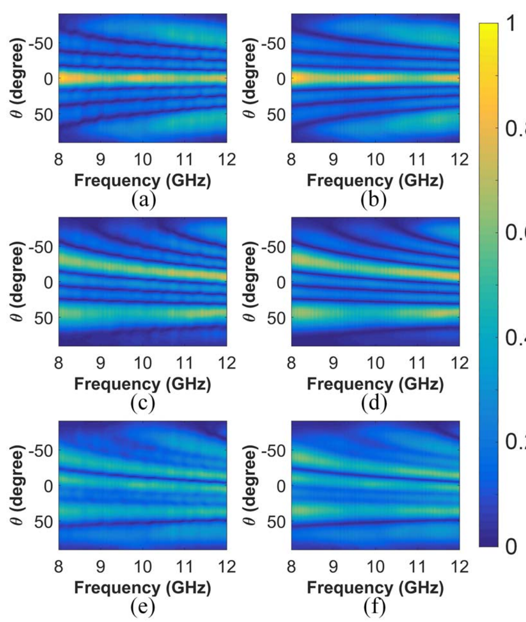

Fig. 4. Two-dimensional system responses obtained by (a), (c), and (e) direct measurements and (b), (d), and (f) the wideband-generalized pattern multiplication approach with (a) and (b) 0°-, (c) and (d) 45°-, and (e) and (f) none-main lobe TTD configurations.

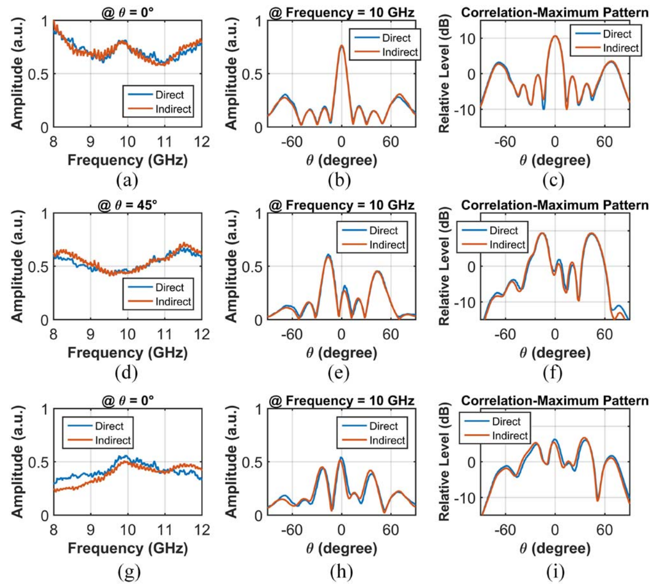

Fig. 5. Details of the system responses in Fig. 4 and the calculated CMPs with (a)–(c) 0°-, (d)–(f) 45°-, and (g)–(i) none-main lobe TTD configurations.

are calculated under a linear frequency-modulated (LFM) feeding with a 10 GHz center frequency and a 3 GHz bandwidth. As can be seen, the results achieved by the wideband-generalized pattern multiplication approach match well with the directly measured ones, however, some small deviation still exists. This is mainly caused by the differences in the radiation features of the four antennas in the array, i.e., the second term in Eq. (2). Since the deviation is negligible in general, the proposed wideband-generalized pattern multiplication approach is valid so that the performance evaluation of the optical beamforming-based wideband antenna array can be conducted using only a small anechoic chamber.

Then, we investigate the sensitivity of the CMP to the distortion of the transmitted signal. For this purpose, the grating lobe of a 16-element, 3 cm spacing array with a main lobe oriented to 45° is numerically studied using both the IAP and the proposed CMP. For simplicity, we assume that the feeding signals are ideally delayed in the OBFN and the antennas in the array are frequency-independent, isotropic, and identical. The array is fed by LFM signals with a center frequency of 10 GHz, a time duration of 50 ns, and different instantaneous bandwidths of 0–4 GHz. Similar to Figs. 4(c) and 4(d), a grating lobe in the system response would be observed around −17°. In addition, the precise position of the grating lobe changes with the feeding frequency, which indicates that if a wideband feeding is applied, only some of the frequency components would be radiated to −17°. Thus, the received signals at −17° would be severely distorted, as the envelopes shown in Fig. 6(a), in which the only distortionless signal is the one under the 10 GHz single tone (0 GHz bandwidth) feeding. The distortion should be mapped to the power levels of the IAP and CMP at −17°. As

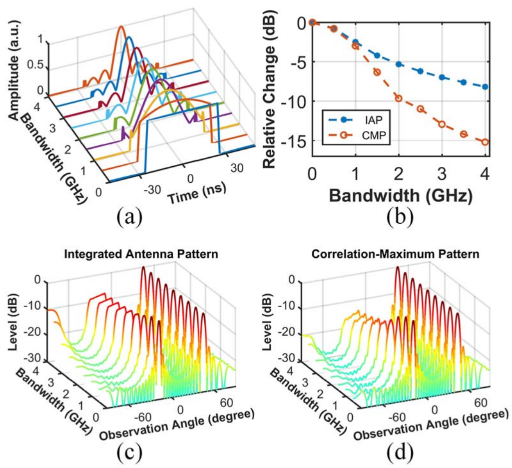

Fig. 6. Signal distortion at a grating lobe of $-17°$ and the corresponding IAP and CMP. (a) Envelopes of the received signals at $-17°$ under different feeding bandwidths; (b) relative changes of the IAP and CMP at $-17°$; and the corresponding (c) IAP and (d) CMP.

can be seen in Figs. 6(c) and 6(d), the values of both of the two kinds of patterns at $-17°$ decreases with the increasing bandwidths, but a more obvious reduction can be found in the CMP. Relative changes of the IAP and CMP at $-17°$ under LFM feedings with different bandwidths are summarized in Fig. 6(b). The CMP, which utilizes the maximal output of a correlation receiver, is more sensitive to the signal distortion induced by the optical beamforming system. In the system where wideband feedings are applied to suppress grating lobes[14,15], the CMP could enable a better suppression ratio under the same feeding condition, as depicted in Figs. 6(c) and 6(d).

In conclusion, a method to evaluate the performance of an optical beamforming-based wideband antenna array is proposed with the wideband-generalized pattern multiplication approach and correlation reception. With the frequency-dependent array factor and the CMP, more comprehensive and intuitive information on the radiation characteristic of an array fed by different wideband signals, which feature the optical beamforming, could be provided for further analysis and evaluation.

This work was supported in part by the NSFC Program (Nos. 61422108 and 61527820), the Jiangsu Provincial Program for High-level Talents in Six Areas (No. DZXX-034), the "333 Project" of Jiangsu Province (BRA2015343), and the Fundamental Research Funds for the Central Universities.

References

1. W. Ng, A. A. Walston, G. L. Tangonan, J. J. Lee, I. L. Newberg, and N. Bernstein, J. Lightwave Technol. **9**, 1124 (1991).
2. S. Pan, D. Zhu, S. Liu, and K. Xu, IEEE Microwave Mag. **16**(8), 61 (2015).
3. S. Pan, D. Zhu, and F. Zhang, Trans. Nanjing Univ. Aeronaut. Astronaut. **31**, 219 (2014).
4. B. Ortega, J. Mora, and R. Chulia, IEEE Photon. J. **8**, 1 (2016).
5. X. Ye, F. Zhang, and S. Pan, Opt. Lett. **41**, 3956 (2016).
6. Z. Cao, F. Li, A. C. F. Reniers, C. W. Oh, H. P. A. V. D. Boom, E. Tangdiongga, and A. M. J. Koonen, IEEE Photon. Technol. Lett. **26**, 575 (2014).
7. Y. N. Wijayanto, A. Kanno, T. Kawanishi, H. Murata, and Y. Okamura, in *2015 10th European Microwave Integrated Circuits Conference (EuMIC)*, 289 (2015).
8. R. D. Esman, M. Y. Frankel, J. L. Dexter, L. Goldberg, M. G. Parent, D. Stilwell, and D. G. Cooper, IEEE Photon. Technol. Lett. **5**, 1347 (1993).
9. Y. Liu, J. Yang, and J. Yao, IEEE Photon. Technol. Lett. **14**, 1172 (2002).
10. C. G. H. Roeloffzen, L. Zhuang, C. Taddei, A. Leinse, R. G. Heideman, P. W. L. van Dijk, R. M. Oldenbeuving, D. A. I. Marpaung, M. Burla, and K. J. Boller, Opt. Express **21**, 22937 (2013).
11. X. Ye, F. Zhang, and S. Pan, Opt. Express **23**, 10002 (2015).
12. T. Tatoli, D. Conteduca, F. Dell'Olio, C. Ciminelli, and M. N. Armenise, Appl. Opt. **55**, 4342 (2016).
13. M. I. Skolnik, *Radar Handbook*, 3rd ed (McGraw-Hill, 2008).
14. V. Sipal, D. Edwards, and B. Allen, in *IEEE International Conference on Ultra-Wideband (ICUWB)*, 236 (2012).
15. X. Ye, Y. Zhang, and S. Pan, in *Proceedings of 2015 International Conference on Optical Communications and Networks (ICOCN)*, 657 (2015).
16. Z. Cao, Q. Ma, A. B. Smolders, Y. Jiao, M. J. Wale, C. W. Oh, H. Wu, and A. M. J. Koonen, IEEE J. Quantum Electron. **52**, 0600620 (2016).
17. R. Bonjour, M. Singleton, S. A. Gebrewold, Y. Salamin, F. C. Abrecht, B. Baeuerle, A. Josten, P. Leuchtmann, C. Hafner, and J. Leuthold, IEEE J. Quantum Electron. **52**, 1 (2016).
18. H. Subbaraman, M. Y. Chen, and R. T. Chen, J. Lightwave Technol. **26**, 2803 (2008).
19. P. Wu, S. Tang, and D. E. Raible, Opt. Express **21**, 32599 (2013).
20. R. Rotman, O. Raz, S. Barzilay, S. R. Rotman, and M. Tur, IEEE Trans. Antennas Propag. **55**, 36 (2007).
21. R. C. Qiu, IEEE J. Sel. Areas Commun. **20**, 1628 (2002).
22. C. A. Balanis, *Antenna Theory: Analysis and Design*, 3rd ed (Wiley, 2005).
23. H. R. Rideout, J. S. Seregelyi, and J. Yao, J. Lightwave Technol. **25**, 1761 (2007).
24. Y. Anliang, Z. Weiwen, L. Shuguang, and C. Jianping, IEEE Photon. J. **6**, 1 (2014).
25. D. Lamensdorf and L. Susman, IEEE Antennas Propag. Mag. **36**, 20 (1994).
26. IEEE Antenna Standards Committee, ANSI/IEEE Std **149**, 1 (1979).